The case for considering polarization in the interpretation of electrical and electromagnetic measurements in the 3 kHz to 3 MHz frequency range

Alain Tabbagh, Fayçal Rejiba, Cécile Finco, Cyril Schamper, B. Souffaché, C. Camerlynck, J. Thiesson, D. Jougnot, A. Maineult

The case for considering polarization in the interpretation of electrical and electromagnetic measurements in the 3 kHz to 3 MHz frequency range.

A.Tabbagh[1], F. Rejiba[2], C. Finco[1], C. Schamper[1], B. Souffaché[1], C. Camerlynck[1], J. Thiesson[1], D. Jougnot[1], A. Maineult[1]

[1]Sorbonne Université, CNRS, EPHE, UMR7619, Métis, 4 place Jussieu F-75252, Cedex 05 Paris, France

[2] Université de Rouen Normandie - UMR CNRS 6143 M2C, place Emile Blondel 76821 Mont Saint Aignan cedex, FRANCE

Abstract

Usually, *in-situ* electrical polarisation measurements (in geophysical prospection referred to as Induced Polarization (IP), or Spectral Induced Polarization (SIP)) have been carried out at frequencies below 1 kHz. These techniques have been used mainly for mining exploration, followed by a larger panel of environmental applications. However, in this ultra and extremely low frequency domain, the duration of each individual measurement is long: typically several tens of minutes for a single full SIP spectrum down to the mHz range. This restriction makes it unrealistic to implement high-density measurement mapping campaigns over large areas, which would otherwise be possible at higher frequencies. In the intermediate frequency range [3 kHz – 3 MHz], laboratory studies of soil and rock samples have shown that they can be strongly polarized notably in the presence of clays, and this property has been confirmed by several *in-situ* mapping experiments using electromagnetic induction (EMI) in the time and frequency domains (FDEM and TDEM), as well as by the electrostatic method (often named Capacitive Coupled Resistivity or CCR). The present paper recalls these results

in an effort to promote polarisation measurements at intermediate frequencies, and to emphasize the importance of measuring this phenomenon.

Key words: electrical polarisation, permittivity, [3 kHz – 3 MHz] frequency range

1.-Introduction

For more than a century, electrical resistivity/conductivity has played a crucial role in near-surface geophysics (Jakosky 1940), for both large surface mapping and localised tomographic/sounding studies based on the measurement of this property. Reference books dealing with the electrical and electromagnetic methods themselves (Keller & Frischknecht 1966, Nabighian ed. 1988 and 1991) and describing different fields of application have contributed to the development of their physical and theoretical foundations and provided numerous practical examples (Scollar et al. 1990, Rubin & Hubbard 2005, Sharma 2008, Dentith & Mudge 2015). Since the seminal work of Archie (1942), considerable research has been devoted to the analysis of several specific parameters - porosity, clay content, water saturation, water mineralization, etc… - affecting the electrical resistivity (e.g. Glover 2015). Various applications, ranging from mining exploration to precision farming can benefit from airborne and ground surveys of this property, over large surface areas. Extensive review papers can be found in the literature, as for example by Pellerin (2002) or Doolittle & Brevik (2014) in the case of near-surface applications. However, as the use of induction electromagnetic methods is commonly limited to electrical resistivity alone, they do not provide a full description of the electrical response of near surface rocks and soils. The determination of their polarisation properties can also be considered, as one cannot *a priori* exclude unknown but possibly valuable information.

Polarisation phenomena were observed very early, in both surface and logging measurements, and Schlumberger (1920) coined the term ‘polarisation provoquée’ (“provoked polarisation” in English) which was later (with a possible confusion with the electromagnetic induction) changed in English to ‘induced polarisation’ (IP). During the 50’s the IP method was applied in time domain measurements (Bleil 1953), and encountered considerable success in ground prospection campaigns applied to mining, as it was able to reveal disseminated mineralization (mainly semiconductor sulphides, e.g. Pelton et al. (1978)). However, even in the absence of minerals, researchers became aware of the role played by clay in IP, including mixtures of clay and coarser particles (Vaquier et al. 1957, Okay et al. 2014). Over the last thirty years, significant developments were achieved on the role of the clay and of the fluid characteristics on the IP signal in the context of groundwater and environmental studies (e.g. Luo and Zhang 1998, Kemna et al. 2012, Binley et al. 2015). Various laboratory studies and field exploration campaigns have been reported, and theoretical models have been proposed. The latter, in particular, established links between electrical polarisation and hydraulic properties (Börner et al. 1996, Revil & Florsch 2010, Fiandaca et al. 2019). Field measurements were performed mostly in the time domain, by measuring the voltage decay after cut-off, over a period ranging from one second to several minutes. However, frequency domain measurements made it possible to gain a better understanding of the frequency dependence of IP (the spectral IP, SIP). Regular workshops allowed the IP community to report on-going research, to publish in special issues, of which the most recent were edited by Camerlynck, Chauris, Maineult and Schmutz (2015 and 2016), Fiandaca, Flores Orozco and Hördt (2017) and by Ntarlagiannis, Wu and Ustra (2019).

IP requires significantly long measurement periods: most frequency domain laboratory studies are carried out over the [1 mHz -1 kHz] frequency range, field measurements last for several minutes per point if such low frequencies are included. This requirement limits complete field studies of IP to fixed point measurements, compatible with 1D soundings. Current electrical resistivity tomography (ERT) acquisition devices used for IP limit the practical frequency range above 1 Hz and below 100 Hz, , but as the number of periods necessary for a good staking controls in the field the progression speed of towed instruments, such frequencies do not match with rapid motion. In order to overcome this limitation, shorter measurement times and higher frequency ranges are needed. Adding higher frequencies to classical IP field investigations will also give access to potential new information (identification of relaxation phenomena with shorter time constant for example) and to a better characterisation of known IP phenomena.

There also exists specific *in-situ* difficulties associated with galvanic IP measurements: ground dependent EM coupling between cables or electrode polarisation (Bhattacharyya and Morrison 1963, Pelton et al. 1978, Kelter et al. 2018). In the [3 kHz – 3 Hz] frequency range these specific difficulties can be overcome by using other measurement principles: magnetic sensors (coils) (Simon et al. 2019) and capacitive poles (Grard and Tabbagh 1991). If one uses metallic electrodes (or liquid electrodes) inserted in the ground one has both a capacitance and a resistance thus a phase shift and significant risk of phase rotation if one of the two characteristics changes, while if one only uses capacitances there is no phase shift and the only difficulty is linked with the relative magnitude of the capacitance at the poles and at the feeding wire (but the leaks are proportional to the capacitances and a model can be performed), poles are only required to present significantly higher capacities than feeding wires

The range of permittivity and conductivity values relevant to Ground Penetrating Radars (GPR) and Time Domain Reflectometry (TDR) applications, have been well documented at frequencies above 30 MHz, and electrical polarisation is usually interpreted in terms of the orientation of polar water molecules. However, little is known between SIP and

GPR frequency ranges. At frequencies in the [3 kHz – 3 MHz] interval, which includes VLF (Very Low Frequency), LF (Low Frequency) and MF (Medium Frequency) measurements, a small number of field observations and tests have been carried out, using three different techniques: Time-Domain Electromagnetics (TDEM), Frequency-Domain Electromagnetic induction (FDEM), and the electrostatic method (Capacitive Coupled Resistivity, CCR). However, with all these techniques the measured responses are usually dominated by the electrical conductivity and the polarisation part is most often neglected. Nevertheless a larger number of both laboratory and field experiments are needed to evaluate the validity of this choice. An accurate evaluation the influence of electrical polarisation would permit a better understanding of its magnitude in various field contexts.

At the macroscopic scale, electrical polarisation corresponds to a situation in which the barycentre of the positive charges does not coincide with the barycentre of the negative charges. At the microscopic pore/grain scales, different processes with different relaxation geometric scales and time constants limit the free displacement of electric charges. Although their detailed classification (Kemna et al. 2012) could be questioned, one can cite: electrode polarisation, membrane polarisation (Marshall and Madden 1959), electrochemical polarisation, interfacial polarisation/diffuse layer polarisation (Revil 2013), and Maxwell-Wagner polarisation (Chen and Or 2006). Depending on the frequency and temperature ranges involved, all of these processes can contribute to the magnitude of the polarisation and can add together so that it could be difficult to single one out and a regular decrease with frequency can be often observed. It must also be underlined that anisotropy in the shape of the polarized volume plays a major part in the magnitude of their moment (Tabbagh et al. 2009).

In a first step towards the assessment of polarisation in the [3 kHz – 3 MHz] frequency range and in view of a better interpretation of EMI or CCR surveys, the present paper provides an overview of published experimental results, at both field and laboratory scales, and in both time and frequency domains.

Part of these experimental results were collected during the course of laboratory SIP experiments, at frequencies of 10 kHz or higher. The considered published results serve as a basis to illustrate the global magnitude of polarisation and conductivity values without being able to identify the different polarisation processes. In an effort to focus this study on common rocks and soils, we do not consider measurements carried out on media containing electronic conductor/semiconductor minerals (oxides, sulphides, metallic particles or graphite).

2.-How should the electrical polarisation be expressed?

In the Maxwell-Ampère equation, the electrical polarisation is represented by the displacement currents. In the frequency domain this can be written:

$$curl\ H = (\sigma_0 + i\omega\varepsilon)E \qquad (1),$$

where E is the electric field, H is the magnetic field, σ_0 is the direct current electrical conductivity, ω is the angular frequency ($\omega = 2\pi f$), $i = \sqrt{-1}$, and ε is the dielectric permittivity. Although this last property describes the dielectric behaviour, in order to take the dielectric losses into account it must be considered complex quantity: $\varepsilon = \varepsilon' - i\varepsilon''$. Here, the imaginary term has the same phase as the motion of free carriers (direct current conductivity, σ_0), from which it cannot be experimentally distinguished. The measured conductivity thus corresponds to: $\sigma' = \sigma_0 + \omega\varepsilon''$, which leads to the Maxwell-Ampère equation being written as:

$$curl\ H = (\sigma_0 + \omega\varepsilon'' + i\omega\varepsilon')E = (\sigma' + i\omega\varepsilon')E \qquad (2)$$

These properties can be also expressed in the form of a complex conductivity ($\sigma' + i\sigma''$) or a complex resistivity ($\rho' - i\rho''$), leading to the following correspondences: $\sigma' = \sigma_0 + \omega\varepsilon''$ and $\sigma'' = \omega\varepsilon'$.

In several publications authors usually refer to a formula derived from the Cole-Cole (1941) model to describe polarisation phenomena (e.g. Pelton et al. 1978):

$$\rho(\omega) = \rho_0 \left[1 - m \left(1 - \frac{1}{1 + (i\omega\tau)^c} \right) \right] \quad (3)$$

where ρ_0 is the direct current resistivity, m is the chargeability and c expresses the enlargement of the relaxation constant (τ) distribution. Note that Eq. (3) is an empirical representation of the polarization mechanisms occurring in geological media, but other empirical models exist, among which multiple or generalized Cole-Cole (see Ghorbani et al. 2009), or constant phase angle model (see for instance Dias (2000) for an extended model collection).

In the following text, in an effort to homogenise and clarify the representation of polarisation and in agreement with other researcher approaches (Knight and Endres (2005), Revil (2013), Loewer et al. (2017)), we regroup all the different polarization mechanisms that can contribute and we express the electrical polarisation in terms of a real effective parameter, the relative permittivity ε_r, defined by $\varepsilon' = \varepsilon_0\varepsilon_r$ (ε_0 being the permittivity in vacuum, $\varepsilon_0 = 8.854 \times 10^{-12}$ Fm^{-1}). Consequently, when considering the published results expressed by the imaginary part of the conductivity we introduce $\varepsilon_r = \frac{\sigma''(\omega)}{\omega\varepsilon_0}$, and when they are expressed by equation (3) we identify $\rho(\omega)$ with $\frac{1}{\sigma' + i\omega\varepsilon_0\varepsilon_r}$. In the following text this relative effective permittivity is for sake of simplicity denominated permittivity, we also use the term imaginary part of the permittivity for $\varepsilon''/\varepsilon_0$.

3. Looking first at simple experimental cases

As introductive illustrations of both the magnitude and the frequency dependence of the permittivity we present in Figure 1a and b the experimental results obtained in laboratory for one soil sample and one rock sample in the [100 Hz – 10 MHz] range using a capacitive cell and a vector multi-meter (PSM 1735, NumetricQ, Ltd). The cell dimensions are, Figure 1c, 19 x 160 x 160 mm^3.

The soil is a clay loam coming from the A horizon of the 'Jardin du Roy' in Paris. This material is indeed complex, where beside mineral grains exist a lot of biological active and residual elements but the presence of a soil layer is usual in geophysical surveys. It has a high porosity, n=0.481 (bulk density 1.34 $g.cm^{-3}$). When dried, at 105°C for 24 hours, the real part of the permittivity equals 3 over the whole frequency range in agreement with the Topp et al. (1980) equation. In that soil sample the drying has eliminated all the polarisation mechanisms except the atomic polarisation of solid grains. The presented measurements have been achieved at a high volumetric water content: θ=0.446 (quasi saturation). One can observe (Figure 1a) that the imaginary part is linearly decreasing with frequency, the slope corresponding to a DC conductivity of 21.6 $mS.m^{-1}$ thus to 46 Ω.m (thin line). The real part has very high values in low frequency as it starts from 9 x 10^5 at 100 Hz, and reaches 4 000 at 3 kHz. Its linear decrease fits with a Jonscher's exponent of -1.45 (Jonscher 1977). Such a regularity in the decrease corresponds to a large distribution of relaxation times. Higher frequency values agrees relatively well with the Topp et al. formula: for θ=0.446, ε_r=29. The curves corresponding to the modelling expression,

$$\varepsilon_r = (9\ 10^5\ (\omega/\omega_0)^{-1.45} + 29 - i\ 0.0216/(\omega\varepsilon_0)) \quad (4),$$

are drawn by a thin continuous lines in the Figure 1a, ω_0 being the angular frequency corresponding to 100 Hz.

The rock sample is a Lutetian limestone extracted from the Saint Pierre Aigle quarry (Aisne, France). It contains calcite, 85% in weight, sand 10% and a few percent of phyllosilicates (clay). The open porosity *n* equals 0.18. The results presented in Figure 1b are measured when the sample is dry, θ=0.017, and the conductivity is too low to be measurable. In addition to the high frequency permittivity behaviour, one can observe a unique relaxation process which fits the following expression (thin lines in Figure 1b),

$$\varepsilon(\omega) = \frac{\Delta\varepsilon}{1+(i\omega\tau)^{c}} + \varepsilon_h' - i\varepsilon_h'' \qquad (5),$$

where $\Delta\varepsilon$ =28, the real part of the high frequency permittivity ε_h' = 4.5, its imaginary part equals ε_h'' = 0.5, c =0.65 and τ =1.75 µs.

In this second sample, the behaviour of the permittivity is very different in amplitude and in frequency dependence from that of the moist soil, but even this dry rock sample has a real part of the permittivity staying above 30 between 100 Hz and 10 kHz, significantly higher than 4.5 at high frequencies.

4.-Published effective permittivity values in laboratory

4.1 Experiments covering the [3 kHz – 3 MHz] frequency range

In order to understand in-field observations made at ground surface or by means of well logging, and to assess the different hypotheses that can be proposed to interpret the data, various laboratory studies have been carried out on both natural and synthetic samples. Unfortunately, there are more published results derived from laboratory studies than from field campaigns. Several studies have covered a wide frequency range, and the results of some are given in Table 1. It can be observed that clayey formations have permittivity values above hundred or thousand between 10 and 100 kHz.

4.2 Values determined at 10 kHz by SIP experiments

SIP gave rise to a large number of laboratory studies, designed to assess the roles played by minerals, their grain size distribution, as well as their fluid nature and content. Several different models have also been tested in the context of these studies, some of which were carried out at frequencies of several tenths of a kilohertz, allowing the permittivity to be determined at 10 kHz (Table 2). Again values of permittivity above 1000 are reported for clayey formations.

5.-Published *in-Situ* data

5.1 Electrostatic measurements (CCR)

This method can be seen as a generalization of the DC resistivity, where the injection electrodes are replaced by an open capacitor and the voltage electrodes by another open capacitor (Grard and Tabbagh 1991, Tabbagh et al. 1993, Kuras et al. 2006). To reduce the pole impedances, the transmitted frequency(ies) must in practice be larger than or equal to 10 kHz. By adopting 100 kHz as the upper frequency limit imposed by the induction effect (Benderitter et al. 1994, Tabbagh and Panissod 2000), an adequate depth of investigation is achieved for most engineering and environmental applications.

Table 3 summarises the ranges of resistivity and permittivity obtained following the acquisition of profile or map data series.

5.2 Electromagnetic frequency domain measurements

Is it possible to measure IP using an inductive system, which would pave the way to direct and large ground and airborne applications? This old question (Hohmann et al. 1970) led to a series of studies that concluded negatively, although these were carried out using simulations and experiments limited to 1.5 kHz for transmitter coil - receiver coil instrument configurations. More recently, some *in situ* experiments have been performed at higher frequencies, using both helicopter-borne and ground-based devices (Table 4) and the coil-coil configuration gave reliable results even at medium frequencies (Kessouri et al. 2016). For FDEM measurements using uniform primary fields, radio-magnetotellurics (RMT) or wave-tilt measurements, the influence of the electrical polarisation has been considered in theory (Grossley 1981) with permittivity values as high as 200 (Sinha et al 1977) but unfortunately the published experiments are limited to very high resistive areas (permafrost and/or crystalline basement) where the permittivity remains below 10 (Kalscheuer et al. 2008).

5.3 TDEM measurements

In principle, TDEM measurements (Nabighian and Macnae 1988) correspond to an extended frequency range, and, as the cut-off time can be as short as 4 µs (Thiesson et al. 2007, Auken et al. 2019), the frequency range considered in the present review corresponds to the early time-domain samples but IP effects can also be observed at late times. The presence of electrical polarisation is observed as an unexpected cancellation of monotonicity in the decrease of the step and impulse responses by reference to what would be expected with the same transmitter/receiver configuration when only conductivity and magnetic viscosity are considered. This phenomenon has been observed since the 70's (Lee 1975), and can only be explained by electrical polarisation (Weidelt 1982). In some cases, the authors were able to check these observations by direct current IP measurements and/or by Cole-Cole modelling.

The corresponding permittivity values, listed in Table 5 below, are estimated from the following equation: $\varepsilon_r = \frac{1}{\omega\varepsilon_0}\mathrm{Im}(\frac{1}{\rho(\omega)})$.

6- General appraisal: amplitude of the polarisation response and relation with conductivity

An overview of the permittivity and resistivity variations is synthetized in Figure 2. Although these results do not give an exhaustive list of the experimental studies reported in the literature, they are sufficient to establish what the electrical polarisation looks like in the [3 kHz – 3 MHz] frequency range.

(1) The magnitude of the electrical polarisation expressed in ε_r can exceed 10 000. It is certainly higher than that observed in the range of frequencies used for GPR/TDR, as summarized by the Topp et al. (1980) cubic formula;

(2) It can be seen that there is consistency between laboratory (Tables 1 and 2) and field measurements (Tables 3, 4 and 5).

(3) Below approximately 300 Ω.m (above 3.3 $S.m^{-1}$), the permittivity looks inversely correlated with resistivity. It exhibits a high variability at least as strong as that of the resistivity. Figure 2 illustrates this anti-correlation. However points are not grouped along a straight or curved line, but scattered. Consequently a significant part of information existing in permittivity is independent on that existing in resistivity.

(4) As expected, the existence of several relaxation mechanisms with gradually increasing time constants corresponds to a decrease of the polarisation with frequency.

(5) In all tabulated results, clay content and ionic strength contribute dominantly to polarisation.

Figure 3 plots the product $\varepsilon_0\varepsilon_r\omega$ as a function of σ, derived from laboratory samples. It can be seen that the samples can be divided into two distinct groups, depending on the presence (higher conductivity) or absence (lower conductivity) of clay. In the first group, most of the data points lay between the lines indicating a contribution of 0.1 and 0.01 of the permittivity relatively to the conductivity. This shows that although conductivity dominates the response, the permittivity responses should also be taken into account. In the second group, the permittivity responses clearly dominate the results. It is thus always necessary to consider both responses.

Tables 1 to 5 reveal that, when the measured resistivity is high, its decrease as a function of frequency due to the presence of dielectric losses, $\omega\varepsilon''$, is more easily observable. In cases where the dielectric losses contribution is significant, it would be useful to compare these frequency-dependent measurements with the direct current resistivity, in the field as well as in the laboratory.

7 Implications for field measurements

It is clear that any processing of field data should consider the polarisation processes independently from the usual conduction processes in the [3 kHz – 3 MHz] frequency range where short measurement durations open the way to high density surveys. In this range the different electrical methods can be split in in three groups: the coil – coil EMI methods, the EMI methods using distant sources, and the electrostatic method (CCR). In the first group, for lower frequencies, measurement interpretation may be even more complicated by the influence of the magnetic properties. Thus, two situations can be considered: in the first, the method is not sensitive to magnetic properties, which may intervene in the second situation.

7.1 In absence of magnetic property influences

In the first situation, given that the Maxwell-Ampère equation states that the conduction the displacement currents are 90 degree's out-of-phase from the conduction ones, the measurement of both in-phase and out-of-phase components (by reference to the primary source signal) is necessary and sufficient to determine the apparent resistivity and the apparent permittivity. Recent electronics devices can easily perform the separation between in-phase and out-of-phase components. The calculation of apparent properties can be done by inversion (Kessouri et al. 2016), by lookup tables (Huang and Fraser 2002) or master curves. Using an inversion procedure is of common use with the electrostatic method (Souffaché et al. 2010, Przyklenk et al. 2016) and with coil –coil FDEM instruments where the frequency is sufficiently high and/or the coil separation sufficiently large (Simon et al. 2019). However, in Magnetotellurics (or Radio MT in the considered range) the influence of the permittivity modifies both the amplitude of the wave impedance and the phase lag between the electric and magnetic fields. Consequently both amplitude and phase sounding curves are distorted and a precise interpretation would be impossible in absence of a phase reference locked on the source of the primary field.

7.2 In presence of magnetic property influences

For small FDEM or TDEM instruments setup, the magnetic properties may have a strong influence. For FDEM, to the best of our knowledge for ground measurements if the magnetic susceptibility do not exceed 10^{-3} SI, the rule of thumb criterion $(f\ L)>10^{6}\ Hz.m$ is relevant (L being the separation between coils) for neglecting the magnetic susceptibility response. If not, several possibilities exist:

(1) in FDEM determine the magnetic susceptibility by moving the frequency at the lower possible values (for example for a metric inter-coil spacing instrument use a frequency around 10 kHz), where the rule of thumb criterion $(f\,L)<3.10^4\ Hz.m$ is relevant to neglect the permittivity response, and in TDEM determine the magnetic viscosity by the late time response.

(2) in FDEM set the height of the instrument in HCP (horizontal coplanar) coil configuration in such way that the magnetic response is negligible as it is known that the magnetic susceptibility response crosses 0 if the instrument altitude equals 0.38*L* (for example if *L*=3.66 m the instrument can be held at a height of 1.4 m)

(3) in FDEM use both HCP and VCP (vertical coplanar) configurations because in the HCP the permittivity in-phase response opposes the magnetic susceptibility while in the VCP it adds (Benech et al. 2016). In all cases, instruments must be carefully calibrated (Thiesson et al. 2014).

The same ideas of combining coil separation and clearance can be applied in TDEM (Finco 2019).

8- Conclusion

We present the results of varied laboratory and field experiments conducted over different material for different objectives. A very brief review of our scope and objectives is in order here.

First, since the magnitude of the permittivity response can be significant (and in some case dominant), exploration geophysicists should not neglect $\varepsilon\omega$ in favour of σ, when implementing EM inductive (both frequency and time domain) and electrostatic exploration methods. In other words, (i) even if present practices are limited to conductivity, taking into account the permittivity will allow a better determination of the conductivity itself which is imperative when simultaneously interpreting different type of conductivity measurement techniques and (ii) there is no reason to *a priori* exclude information.

Second, the measurement and in-field mapping of permittivity may open opportunities for the exploration of a broad range of new types of geophysical information. In the considered frequency range, both conductivity and permittivity depend on the total amount of mobile ions, conductivity corresponding to free motion and permittivity to constrained motions limited by what may oppose to the ion displacements: pore size and throat configuration, disposition, shapes and types of clay platelets, etc…

References

Archie G. E., 1942. The electrical resistivity log as an aid in determining some reservoir characteristics. SPE-AIME Transactions, 146, 54-62.

Auken E., Foged N., Larsen J. J., Lassen K. V. T., Maurya P. K., Dath S. M., Eiskjaer T. T., 2019. tTEM – A towed transient electromagnetic system for detailed 3D imaging of the top 70m of the surface. Geophysics, 84-1, E13-E22.

Benderitter, Y., Jolivet, A., Mounir, A., & Tabbagh, A, 1994. Application of the electrostatic quadripole to sounding in the hectometric depth range. Journal of Applied Geophysics, 31(1-4), 1-6.

Benech C., Lombard P., Réjiba F., Tabbagh A., 2016. Demonstrating the contribution of dielectric permittivity to the in-phase EMI response of soils: example of an archaeological site in Bahrain. Near Surface Geophysics, 14-4, 337-344.

Bhattacharyya, B. K., Morrison, H. F., (1963). Some theoretical aspects of electrode polarization in rocks. Geophysical Prospecting, 11(2), 176-191.

Binley A., Hubbard S. S., Huisman J. A., Revil A., Robinson D. A., Singha K., Slater L. D., 2015. The emergence of Hydrogeophysics improved understanding of subsurface processes over multiple scales. Water Resources Research, 51(6), 3837-3866.

Bleil D. F., 1953. Induced Polarisation: a method of geophysical prospecting. Geophysics, 18, 636-661.

Börner F. D., Schopper J. R., Weller A., 1996. Evaluation of transport and storage properties in the soil and groundwater zone from induced polarization measurements. Geophysical Prospecting, 44, 583-601.

Camerlynck C., Chauris H., Maineult A., Schmutz M. (editors), 2015. Special issue on new trends in induced polarization- Part 1. Journal of Applied Geophysics, 123, 283-344.

Camerlynck C., Chauris H., Maineult A., Schmutz M., (editors), 2016. Special issue on new trends in induced polarization- Part 2. Journal of Applied Geophysics, 135, 375-502.

Chen Y., Or D., 2006. Effects of Maxwell-Wagner polarization on soil complex dielectric permittivity under variable temperature and electrical conductivity. Water Resources Research, 42, W06424.

Cole K. S., Cole R. H., 1941. Dispersion and absorption in dielectrics, I. alternating current characteristics. Journal of Chemical Physics, 9, 341-351.

Dentith M., Mudge S. T., 2015. Geophysics for the Mineral Exploration Geoscientist. Cambridge University Press.

Dias, C. A., 2000. Developments in a model to describe low-frequency electrical polarization of rocks. Geophysics, 65, 437-451.

Doolittle J. A., Brevik E. C., 2014. The use of electromagnetic induction techniques in soils studies. Geoderma, 223-225, 33-45.

Fiandaca G., Flores Orozco A., Hördt A. (editors), 2017. Special issue on induced polarization – Narrowing the gap between theory and observations. Near Surface Geophysics, 15(6).

Fiandaca G., Maurya P. K., Balbarini N., Hordt A., Christiansen A. V., Foged N., Bjerg P. L., Auken E., 2019. Permeability estimation directly from logging-while-drilling Induced Polarization data. Water Resources Research, 54, 2851-2870.

Finco, C., 2019. Étude de l’impact simultané des propriétés électriques, diélectriques et magnétiques du sous-sol sur la mesure géophysique par méthode électromagnétique inductive dans le domaine temporel (TDEM). PhD Thesis, Sorbonne Université, Paris, France.

Ghorbani A., Cosenza P., Revil A., Zamora M., Schmutz M., Florsch N., Jougnot D., 2009. Non-invasive monitoring of water content and textural changes in clay-rocks using spectral induced polarization: A laboratory investigation. Applied Clay Science, 43(3-4), 493-502.

Glover P. W. J., 2015. 11.04- Geophysical Properties of the Near Surface Earth: Electrical Properties, in Treatise on Geophysics (second edition), Elsevier, 11, 89-137.

Grard R., Tabbagh A., 1991. A mobile four electrode array and its application to the electrical survey of planetary grounds at shallow depths. Journal of Geophysical Research, 96-B3, 4117-4123.

Crossley D. J., 1981. The theory of EM surface wave impedance measurements. In Geophysical Applications of Surface Wave Impedance Measurements, Paper no. 81-15, pp. 1–17, editors Collet, L.S. and Jensen, O.G., Geological Survey of Canada.

Hohmann G. W., Kintzinger P. R., van Voorhis G. D., Ward S. H., 1970. Evaluation of the measurement of induced electrical polarization with an inductive system. Geophysics, 35(5), 901-915.

Huang H., Fraser D. C., 2002. Dielectric permittivity and resistivity mapping using high-frequency, helicopter-borne EM data. Geophysics, 67(3), 727-738. Jakosky J. J., 1940. Exploration geophysics. Trija Publishing Company, Newport Beach

Jonscher A. K., 1977. The universal dielectric response. Nature, 267, 673-679.

Kalscheuer T., Pedersen L. B., Siripunvaraporn W., 2008. Radiomagnetotelluric two-dimensional forward and inverse modelling accounting for displacement currents. Geophysical Journal International, 175, 486-514.

Keller G. V., Frischknecht F. C., 1966. Electrical methods in geophysical prospecting, Pergamon press, Oxford.

Kemna A., Binley A., Cassiani G., Niederleithinger E., Revil A., Slater L., Williams K. H., Flores Orozco A., Haegel F-H., Hördt A., Kruschwitz S., Leroux V., Titov K., Zimmermann E., 2012. An overview of the spectral induced polarization method for near-surface applications. Near Surface Geophysics, 10, 453–468.

Kessouri P., Flageul S., Vitale Q., Buvat S., Rejiba F., Tabbagh A., 2016. Medium-frequency electromagnetic device to measure electric conductivity and dielectric permittivity of soils. Geophysics, 81-1, E1-E16.

Kelter M., Huisman J. A., Zimmermann E., Vereecken, H., 2018. Field evaluation of broadband spectral electrical imaging for soil and aquifer characterization. Journal of Applied Geophysics, 159, 484-496.

Knight, R. J. and Endres, A. L., 2005. An introduction to rock physics principles for near-surface geophysics, in Near-surface geophysics. Society of Exploration Geophysicists, pp. 31–70.

Kuras O., Beamish D., Meldrum P. I., Ogilvy R. D., 2006. Fundamentals of capacitive resistivity technique. Geophysics, 71-3, G135-G152.

Lee T., 1975. Sign reversals in the transient method of electrical prospecting (one loop version). Geophysical Prospecting, 23(4), 651-662.

Loewer, M., Günther, T., Igel, J., Kruschwitz, S., Martin, T. and Wagner, N., 2017. Ultra-broad-band electrical spectroscopy of soils and sediments-a combined permittivity and conductivity model, Geophysical Journal International, 210(3), 1360–1373.

Luo Y., Zhang G., 1998. Theory and application of spectral induced polarization. Society of Exploration Geophysicists, Tulsa, OK, USA.

Marshall D. J., Madden T. R., 1959. Induced polarization, a study of its causes. Geophysics, 24(4), 790-816.

Nabighian M. N. editor, 1988. Electromagnetic Methods in Applied Geophysics. Volume 1 Theory, Tulsa, OK, Nabighian M. N. editor, 1991. Electromagnetic Methods in Applied Geophysics. Volume 2 Applications, Tulsa, OK

Nabighian M. N., Macnae J. C., 1988. Time domain electromagnetic prospection method. In Electromagnetic methods in applied geophysics (Nabighian editor), SEG, Vol 2, part A, 427-514.

Ntarlagiannis D., Wu Y., Ustra A. T. (editors), 2019. Special issue: Recent Developments in Induced polarization. Near Surface Geophysics, 17(6).

Okay G., Leroy P., Ghorbani A., Cosenza P., Camerlynck C., Cabrera J., Florsch N., Revil A. 2014. Spectral induced polarization of clay-sand mixtures: Experiments and modeling. Geophysics, 79(6), E353-E375.

Pellerin L., 2002. Applications of electrical and electromagnetic methods for environmental and geotechnical investigations. Surveys in Geophysics 23(2), 101-132.

Pelton W. H., Ward S. H., Hallof P. G., Sill W. R., Nelson P. H., 1978. Mineral discrimination and removal of inductive coupling with multifrequency IP. Geophysics, 43(3), 588-609.

Przyklenk, A., Hordt A., Radi T., 2016. Capacitively Coupled Resistivity measurements to determine frequency-dependent electrical parameters in periglacial environment—theoretical considerations and first field tests. Geophysical Journal International, 206, 1352-1365.

Revil A., 2013. Effective conductivity and permittivity of unsaturated porous materials in the frequency range 1 mHz – 1GHz. Water Resources Research, 49, 306-327.

Revil A., Florsch N., 2010. Determination of permeability from spectral induced polarisation data in granular media. Geophysical Journal International, 181, 1480-1498.

Rubin Y., Hubbard S. S., 2005. Hydrogeophysics. Springer

Schlumberger C., 1920. Etude sur la prospection électrique du sous-sol: Paris, Gauthier-Villars

Scollar I., Tabbagh A., Hesse A., Herzog I., 1990. Archaeological Prospecting and Remote Sensing. Cambridge University Press

Sharma P. V., 2008. Environmental and engineering geophysics. Cambridge University Press.

Sinha A.K., 1977. Influence of altitude and displacement currents on plane wave EM fields. Geophysics, 42(1), 77–91.

Simon F.-X., Tabbagh A., Donati J. C., Sarris A., 2019. Permittivity mapping in the VLF-LF range using a multi-frequency EMI device: first tests in archaeological prospection. Near Surface Geophysics, 17, 27-41.

Souffaché B., Cosenza P., Flageul S., Pencolé J-P., Seladji S., Tabbagh A., 2010. Electrostatic multipole for electrical resistivity measurements at the decimetric scale. Journal of Applied Gophysics, 71, 6-12.

Tabbagh A., Cosenza P., Ghorbani A., Guérin R., Florsch N., 2009. Modelling Maxwell-Wagner induced polarization amplitude for clayed material. Journal of Applied Geophysics, 67, 109–113.

Tabbagh A., Hesse A., Grard R., 1993. Determination of electrical properties of the ground at shallow depth with an electrostatic quadrupole: field trials on archaeological sites. Geophysical Prospecting, 41, 579-597.

Tabbagh A., Panissod C., 2000. 1D complete calculation for electrostatic soundings

Interpretation. Geophysical Prospecting, 48, 511-520.

Thiesson J., Tabbagh A., Flageul S., 2007. TDEM magnetic viscosity prospecting using a Slingram coil configuration. Nera Surface Geophysics, 5, 363-374.

Thiesson J., Kessouri P., Schamper C., Tabbagh A. 2014. Calibration of frequency-domain electromagnetic devices used in near-surface surveying. Near Surface Geophysics, 12-4, 481-491.

Topp G. C., Davis J. L., Annan P., 1980. Electromagnetic determination of soil water content: measurements in coaxial transmission lines. Water Resources Research, 16-3, 574-582.

Vaquier V., Holmes C. R., Kintzinger P. R., Lavergne M., 1957. Prospecting for groundwater by induced polarization. Geophysics, 22(3), 660-687.

Weidelt P., 1982. Response characteristics of coincident loop transient electromagnetic systems. Geophysics, 47(9), 1325-1330.

Figure captions

Figure 1: Example of frequency variation of the permittivity of (a) a clay loam soil (A horizon) sample, (b) the Saint Pierre Aigle limestone: (bold continuous line for the real part, bold dashed line for the imaginary part). The corresponding models (respectively expression (4) and (5)) are in thin continuous lines, (c) capacitive cell and PSM vector multi-meter.

Fig 2: Relationship between the relative permittivity and the conductivity (in Sm^{-1})/resistivity (in Ω.m). For the different tables (left) and for the different frequencies (right).

Fig 3: Laboratory results: comparison between $\varepsilon_0 \varepsilon_r \omega$ (in S m^{-1}) and σ (in Sm^{-1}) values

Table captions

Table 1: Permittivity values in laboratory experiments covering the [3 kHz – 3 MHz] range. (Notations: *a* is the side of a square cell, *e* is the thickness of disk, cylindrical or square cells and *d* is the diameter of cylindrical or disk cell).

Table 2: Permittivity values delivered at 10 kHz by laboratory SIP experiments. (Notations: *e* is the thickness of disk or cylindrical cells and *d* is the diameter of cylindrical or disk cell).

Table 3: Permittivity values obtained by *in-situ* electrostatic measurements.

Table 4: Permittivity values obtained by *in situ* frequency domain measurements.

Table 5: Permittivity values obtained by *in situ* TDEM measurements.

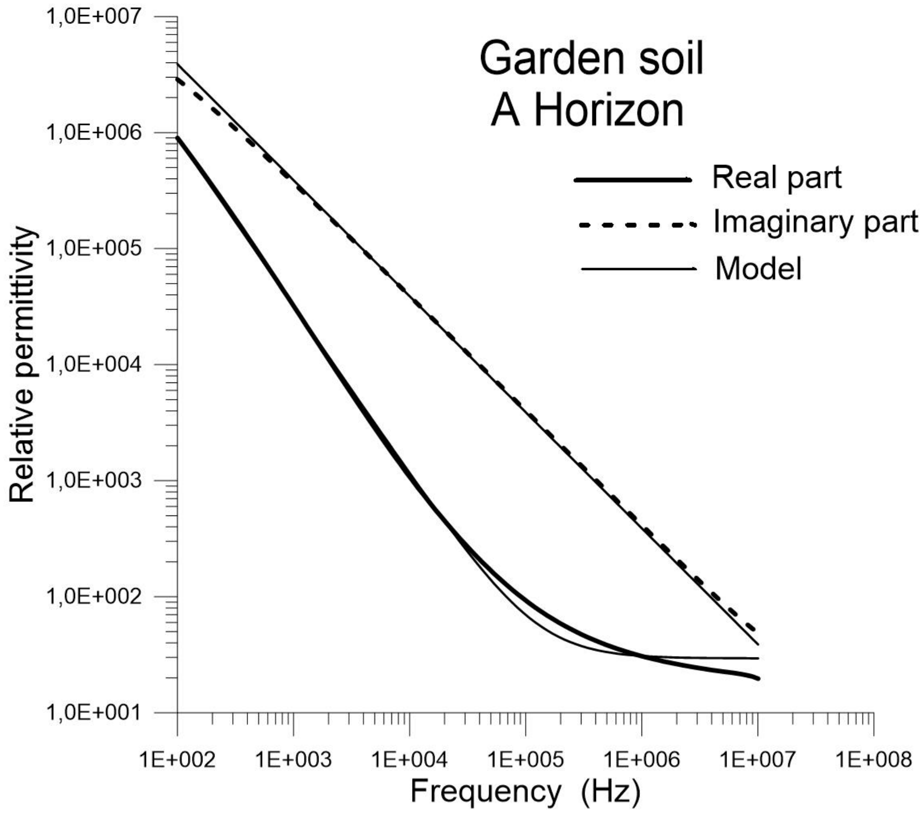

Figure 1a

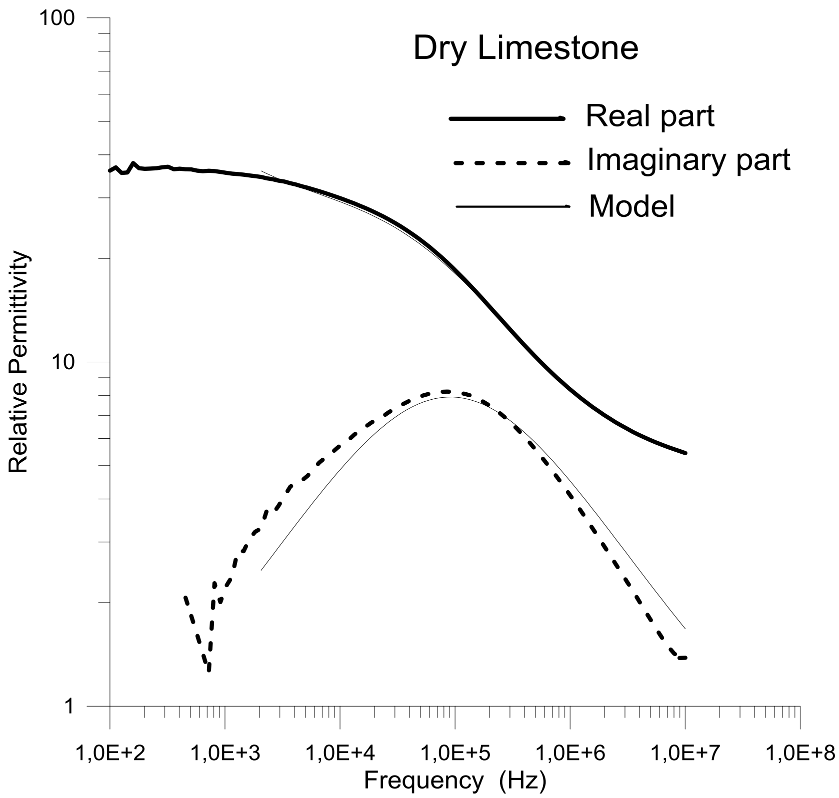

Figure 1b

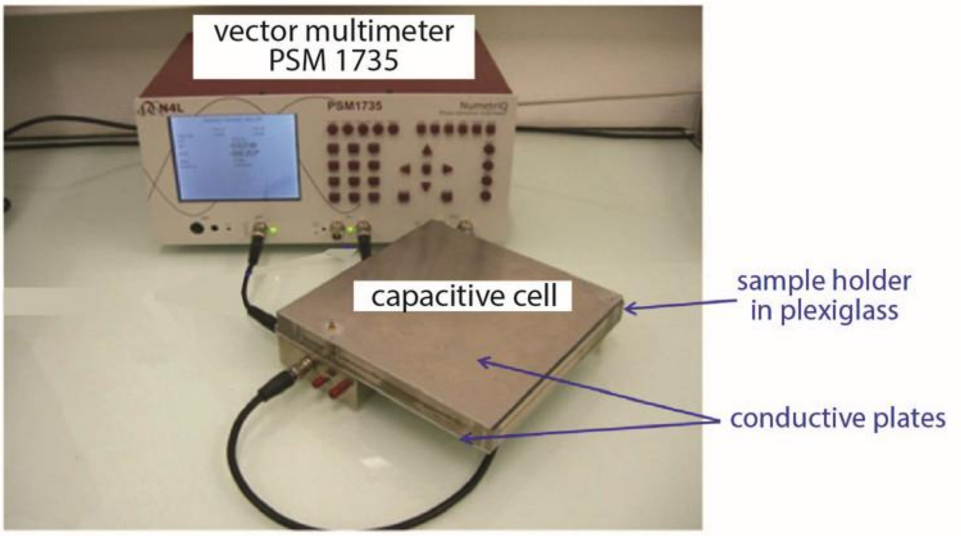

Figure 1c

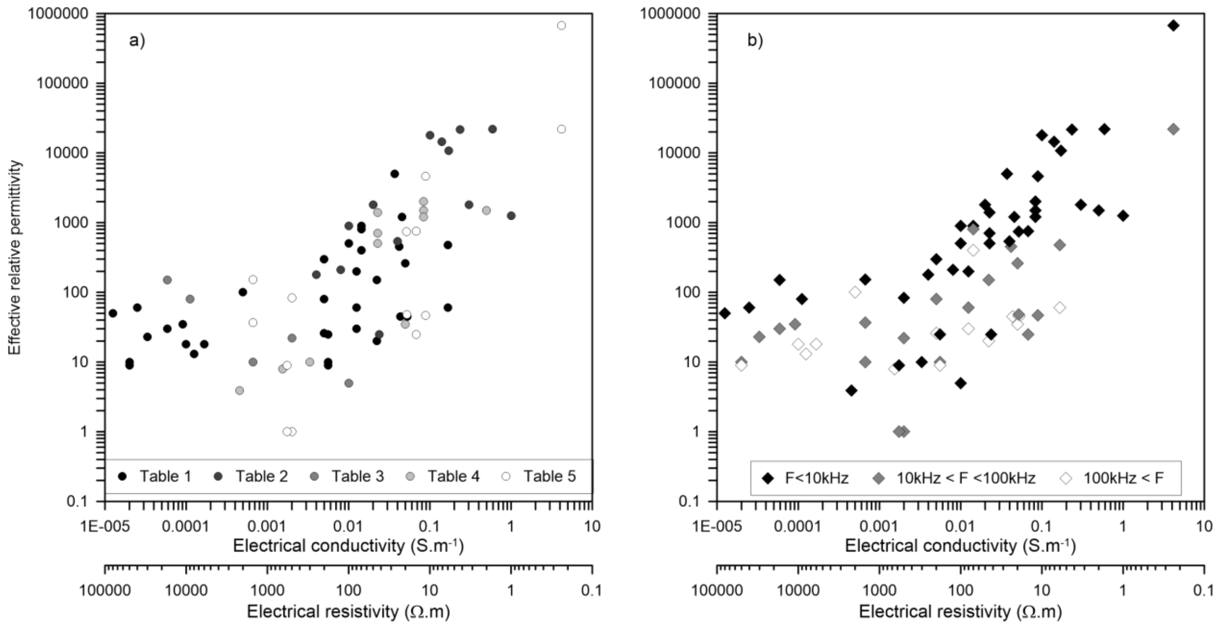

Figure. 2

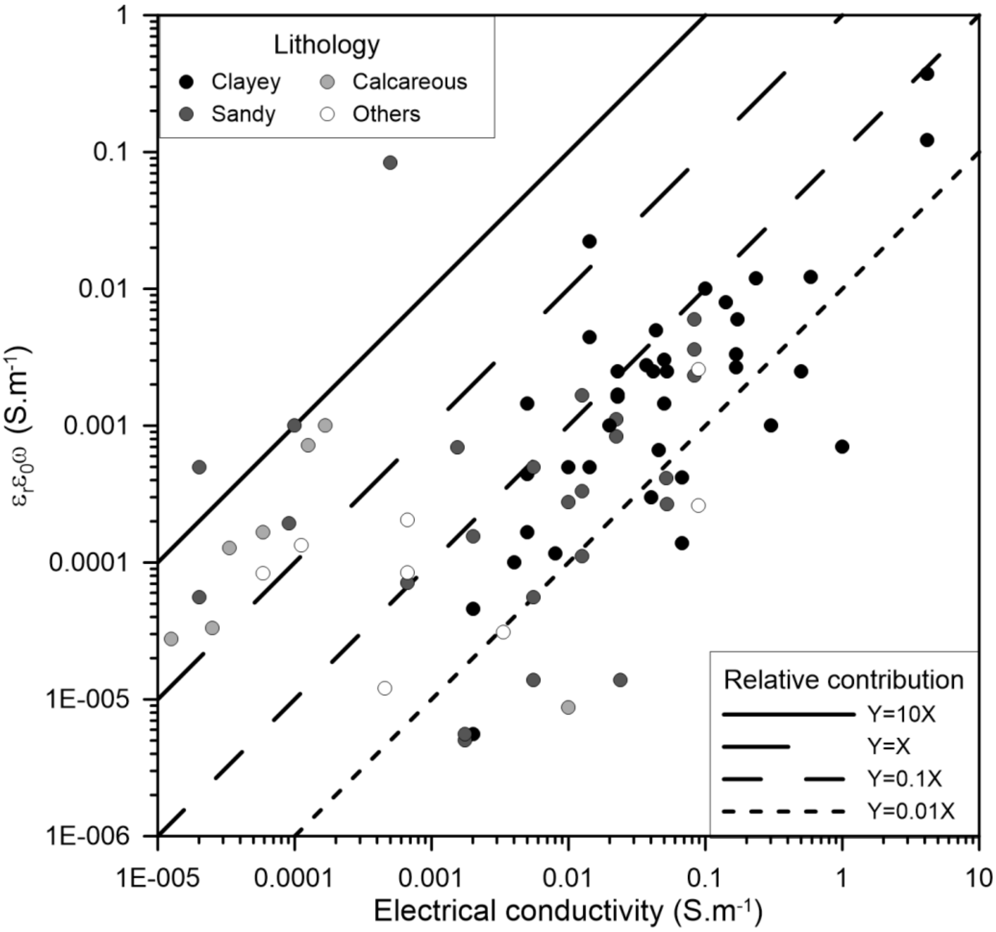
Lithology
Clayey
Calcareous
Sandy
Others
Relative contribution
Y=10X
Y=X
Y=0.1X
Y=0.01X
1
0.1
0.01
0.001
0.0001
1E-005
1E-006
1E-005
0.0001
0.001
0.01
0.1
1
10
Electrical conductivity (S.m-1)
εrε0ω (S.m-1)

Figure. 3

Reference	Sample size and cell	Sample characteristics	Frequency	Electrical resistivity	Relative permittivity
Scott et al. 1967, J.G.R., 72, 5101-5115.	Cylindrical capacitance cell d=2.54 cm e=2.54 cm 2 electrodes	Mancos shale (3.8% volume water content)	10 kHz	200 Ω.m	300.
			100 kHz	200 Ω.m	80.
			1 MHz	200 Ω.m	26.
Kenyon 1984 Journal of applied Physics, 55 ,3153-3159	Coaxial cell	Whitestone calcite saturated with 1.07Ω.m NaCl solution	1 MHz	18 Ω.m	800
Knight & Nur 1987, Geophysics 52(2), 644-654.	Disk-shaped capacitance cell d=5.1 cm e=0.5 cm 2 electrodes	CH66-79 Berea sandstone, Sw=0.36 deionized water	100 kHz	11,000 Ω.m	35.
			1 MHz	10,000 Ω.m	18.
		St Peter's sandstone S_w=0.36 deionized water	100 kHz	50,000 Ω.m	10.
			1 MHz	50,000 Ω.m	9.
Garrouch & Sarma 1994, Geophysics 59(6) 909-917.	Disk-shaped capacitance cell e=3 to 10 mm 2 and 4 electrodes	102 shaly sand brine saturated (8%)	10 kHz	27 Ω.m	5,000.
			100 kHz	24 Ω.m	450.
			2 MHz	23 Ω.m	45.
		144 sandy clay brine, saturated (8%)	10 kHz	Not given	15,000.
			100 kHz		500.
			2 MHz		100.
Tabbagh 1994, Archaeometry, 36, 159-170.	Square capacitance cell a=190 mm e=19 mm 2 electrodes	Sandy clay loam, saturated 43 %	10 kHz	70 Ω.m	900.
			100 kHz	70 Ω.m	800.
			1 MHz	70 Ω.m	400.
		Volcanic sand, saturated 43.6 %	10 kHz	Not given	50.
			100 kHz		25.
			1 MHz		15.
		Porous limestone, saturated 16.5%	10 kHz	Not given	40.
			100 kHz		35.
			1 MHz		25.
Lesme & Frye 2001, J.G.R., 106-B3, 4079-4090	Disk-shaped capacitance cell 2 electrodes	Berea sandstone (68% quartz), saturated (0.01M NaCl)	10 kHz	80 Ω.m	200.
			100 kHz	80 Ω.m	60.
			1 MHz	80 Ω.m	30.
Sternberg & Levitskaya 2001. Radio Science 36(4), 709-719.	Coaxial cell	Avra valley sandy silt with clay, water content10.6%	10 kHz	22 Ω.m	1,200.
			100 kHz	20 Ω.m	260.
			1 MHz	19 Ω.m	45.
		Brookhaven sandy soil, water content 9.75 %	10 kHz	180 Ω.m	25.
			100 kHz	180 Ω.m	10.
			1 MHz	180 Ω.m	9.
Oh & al. 2007, Environ. Geol. 51, 821-833	Disk-shaped capacitance cell d= 70 mm e=2 mm 2 electrodes	Sandy soil, water content 23%	100 kHz	45 Ω.m	150.
			1 MHz	45 Ω.m	20.
		Sandy soil with 10% bentonite, water content 23%	100 kHz	6 Ω.m	480.
			1 MHz	6 Ω.m	60.
Wagner et al. 2011 IEEE Geoscience & Remote Sensing 49-7,	Coaxial cell d=7 and 16 mm length 100mm	Silty clay loam (Unstrut river, Germany) Porosity 0.43, Water content 0.38	10 kHz	9 Ω.m	5,000
			100 kHz	8.5 Ω.m	410
			1 MHz	8 Ω.m	295
Abou El-Anwar & Gomaa, 2013, Geophys. Prospect., 61, 630-644.	Cylindrical, 2 electrodes	sandy lime-mudstone/dolostone	10 kHz	40,000 Ω.m	60.
			100 kHz	17,000 Ω.m	30.
			1 MHz	6,000 Ω.m	18.
		sandy dolomitic bioclastic wackestone-mudstone	10 kHz	80,000 Ω.m	50.
			100 kHz	30,000 Ω.m	23.
			1 MHz	8,000 Ω.m	13.

546 Table 1

Reference	Sample size and cell	Sample characteristics	Electrical resistivity	Relative permittivity 10 kHz
Börner et al. 1993, Geophys. Prosp. 41, 83-98.	Cylindrical d=20mm e=30mm 4 electrodes	KT2 Clay	1 Ω.m	1,260.
		E14 shaly sandstone (σ_w=0.01 S/m)	250 Ω.m	180.
		E6 shaly sandstone (σ_w= 0.002 S/m)	125 Ω.m	210.
		BEN bentonite with brine (σ_w=1 S/m)	1.7 Ω.m	22,000.
		KAO kaolinite with brine (σ_w=1 S/m)	10 Ω.m	18,000.
Breede et al. 2012, Near Surface Geophysics, 10, 479-489	Cylindrical d=8 cm e=10 cm 4 electrodes	Sand/Clay (5%) mixture saturated	100 Ω.m	900.
		Sand/Clay (20 %) mixture saturated	50 Ω.m	1,800.
Okay et al. 2014, Geophysics, 79(6), E353-E375.	Cylindrical d=20 cm e=10 cm 4 electrodes in square array	Saturated, kaolinite with 20% sand σ_w=0.02 S/m	25 Ω.m	540.
		Saturated smectite with 20% sand σ_w=0.02 S/m	3.3 Ω.m	1,800.
Kremer et al. 2016, Geophys. J. Inter. 207, 1303 – 1312.	Cylindrical e=40 cm d=30 cm Rectangular 4 electrode array over a section	Saturated silica sand σ_w=15 mS/m	Not given	234
		Saturated silica sand σ_w=100 mS/m	Not given	1,440.
		Saturated carbonated sand σ_w=15 mS/m	Not given	180.
		Saturated carbonated sand σ_w=100 mS/m	Not given	1,260.
Loewer et al; Geophysical Journal International 210, 1360-1373	Cylindrical cell length 70 mm d=20mm 4 electrodes array	Soil A: moist silty clay water content 0.358	12,6 Ω.m	1,000
		Soil B laterite water content 0.303	100 Ω.m	630
		Soil C humus water content 0.368	63 Ω.m	200
		Obersulzbacher sanstone Formation factor 34 Archie exponent 2.19	100 Ω.m	400
Revil et al. 2017, Water Ressources Research, 53, WR020655	Disk shaped d=7. cm e=2.5 cm 4 electrodes in Wenner array	Peat (AC_0580585123), σ_w=0.031S/m	4.26 Ω.m	21,600.
		Clay (CW_0580586130), σ_w=0.031S/m	7.1 Ω.m	14,400.
		Sandy Clay (AR_1126238AA) σ_w=0.031S/m	5.85 Ω.m	10,800.
Revil et al. 2018 Geophysics, 83(2), E55-E74	Cylindrical 4 electrodes	Low porosity sandstone (Eocene deltaic formation) σ_w=0.11 S/m	42 Ω.m	25.

Table 2

Reference	Array configuration	Soil or rock context	Frequency	Electrical resistivity range	Relative permittivity range
Grard & Tabbagh 1991, J.G.R., 96-B3, 4117-4123.	1m x 1.17m rectangular array	Quaternary alluvial sand	128 kHz	500 – 2500 Ω.m	22. – 60.
Tabbagh et al. 1993, Geophysical Prospecting, 41, 579-597.	1m x 1.17m rectangular array	Sandy soil above rhyolite	128 kHz	1500 – 7000 Ω.m	10. – 200.
Przyklenk et al. 2016 Geoph. J. Int., 206 1352-1365.	Wenner arrays a=1m, 1.5m, 2m	Ice over Triassic limestone in a tunnel	10 kHz	17000 Ω.m	150
			30 kHz	9000 Ω.m	80
Souffaché et al. 2016, Archaeometry, 58-5, 705-721.	0.15m x 0.27m rectangular array	Lutetian calcareous stone in monuments	31.25 kHz	100 – 30000 Ω.m	5 - 10000

Table 3

Reference	Instrument & coil configuration	Soil or geological context	Frequency	Electrical resistivity range	Relative permittivity range
Huang & Fraser 2001, Geophysics, 66(1) 148-157	Helicopter borne Dighem HCP L=6.3 m	Crystalline basement in northern Canada	56 kHz	300 - 120,000 Ω.m	10 - 80.
Huang & Fraser 2002, Geophysics, 67(3) 727-738	Helicopter borne Dighem HCP L=6.3 m	At the center of a shallow lake in Northern Canada	56 kHz	2,800 Ω.m	65
Hodge, 2004, SEG 74th (abstracts), 660-663.	Helicopter born Dighem HCP L=6.3 m	Slave geological province, northern Canada	56 kHz	2,200 – 24,000 Ω.m	3.9 - 17.2
Kalscheuer et al. 2008 Geophysical J. int.,175, 486-514	Tensor RMT	Ävrö Island (Sweden) Granite	14 – 226 kHz	Granite median value50,000 Ω.m	6
Benech et al. 2016 Near Surface Geophysics 14(4) 337-344.	CMD HCP and VCP L=1.28m & 0.71m	Salted clayey soil over a marl weathered substratum	30 kHz	2 - 15 Ω.m	1,500 – 30,000
Simon et al. 2019 Near Surface Geophysics 17, 27-41	GEM-2 HCP L=1.66m	Archaeological site bordering the shore line, Loam	21.03 kHz	12 - 80 Ω.m	2,000 – 4,300
			43.35 kHz	12 - 80 Ω.m	1,500 – 4,000
			89.43 kHz	12 - 80 Ω.m	1,200 – 2,200
Simon et al. 2019 Near Surface Geophysics 17, 27-41	GEM-2 HCP L=1.66m	Archaeological site Loam	21.03 kHz	44 - 700 Ω.m	1,400 – 2,600
			43.35 kHz	44 - 700 Ω.m	700 - 1300
			89.43 kHz	44 - 700 Ω.m	500 - 900
Kessouri et al. 2016 Geophysics 81(1) E1-E16	CE 120 prototype PERP L=1.2m	Clay loam	1.56 MHz	20 - 60 Ω.m	35 - 110
Kessouri et al. 2016 Geophysics 81(1) E1-E16	CE 120 prototype PERP L=1.2m	Sandy alluvial	1.56 MHz	650 – 10,000 Ω.m	8 - 18

Table 4

Reference	TDEM instrument	Local Geology	Cole-Cole interpreted parameters	ε_r 10 kHz	ε_r 100 kHz
Walker & Kojikawasaki, 1988, Geoexploration, 25, 245-254	EM37 400m x 400m central-loop	Permafrost, clay and/or gas hydrates	1000 m first layer ρ_0=1000 Ω.m, m=0.5, τ=0.00069s, c=1.	83.	1.
Flis et al. 1989, Geophysics, 54(4), 514-523	Early time SIROTEM 100m x 100m coincident loop	pelite/sandstone	layer 1 (15m thick): ρ_0=22 Ω.m, m=0.13,τ=0.01s, c=0.25 layer 2: ρ_0=600Ω.m, m=0.05,τ=0.01s, c=0.25	747. 9.	48. 1.
Descloitres et al. 2000, J. App. Geo., 45 1-18 ;	PROTEM 47 100m x 100m Receivers at several offsets	Caldera of Fogo Volcano	60 m first layer ρ_0=10000 Ω.m, m=0.85, τ=0.00002s, c=0.8	153.	37.
Hallbauer-Zadorozhnaya & Bessonov, 2002, EJEEG, 7, 239-264	KARIER 5m x 5m coincident loop	Hydrocarbon contaminated quaternary sand above Albian clay	20 m first layer ρ_0=15 Ω.m, m=0.25, τ=0.00018s, c=1.	4,626.	47.
Antonov & Shein 2008, Russian geology and geophysics, 49, 790-802	100m x 100m Coincident loop	Clay quarry overlain by quaternary alluvium	Second layer between 4 and 48m, ρ_0=16 Ω.m, m=0.073, τ=0.00076s, c=0.53	755.	25.
Hallbauer-Zadorozhnaya et al. 2016, J. App. Geo., 133, 16-24.	Zerotem 50m x 50m central loop	Marine clay	Fourth layer below 59 m ρ_0=0.5 Ω.m, m=0.25, τ=0.0035s, c=1.	7,275.	73.
Finco et al. 2018, Hydrological Processes, 32, 3954-3965	TEM-FAST 25m x 25m coincident loop	Sebkha Kelbia salted wetland	2 m first layer ρ_0=1.5 Ω.m, m=0.84, τ=0.01s, c=0.955	83,300.	926..

Table 5